Research Article | Vol. 27, No. 12 | 10 Jun 2019 | OPTICS EXPRESS 16624
Optics EXPRESS

All-dielectric metamaterial analogue of electromagnetically induced transparency and its sensing application in terahertz range

TIAN MA,[1,5] QIUPING HUANG,[2,3] HONGCHUAN HE,[4] YI ZHAO,[2] XIAOXIA LIN,[2] AND YALIN LU[1,2,3,4,6]

[1]*National Synchrotron Radiation Laboratory, University of Science and Technology of China, Hefei,Anhui, 230026, China*
[2]*Hefei National Laboratory for Physical Sciences at the Microscale, University of Science and Technology of China, Hefei, Anhui, 230026, China*
[3]*Synergetic Innovation Center of Quantum Information & Quantum Physics, University of Science and Technology of China, Hefei, Hefei 230026, China*
[4]*Department of Materials Science and Engineering, University of Science and Technology of China, Hefei 230026, China*
[5]*tianma@ustc.edu.cn*
[6]*yllu@ustc.edu.cn*

Abstract: A novel electromagnetically induced transparency (EIT) all-dielectric metamaterial is proposed, fabricated, and characterized. The unit cell of the proposed metamaterial comprises of two asymmetric split ring resonators (a-SRRs) positioned with a mirror symmetry. The asymmetric nature of a-SRRs results from the length difference of two arcs. Optical properties of the fabricated metamaterial are investigated numerically using finite difference method, as well as experimentally using a terahertz time-domain spectroscopy. The results confirm that the proposed metamaterial exhibits an EIT transparent window in the frequency range around 0.78THz with a Q-factor of ~75.7 and a time-delay up to ~28.9ps. Theoretical investigations show that EIT effects in our metamaterial are achieved by hybridizing two bright modes in the same unit cell, which are aroused by the excitation of magnetic moments. We also confirm that the proposed metamaterial has great potential for sensing applications with high sensitivity and high figure of merit (FOM), which guarantees potential applications in in situ chemical and biological sensing.

1. Introduction

The concept of electromagnetically induced transparency (EIT) was originally used to demonstrate the elimination of absorption within a narrow spectral band due to quantum interference when light propagates through an originally opaque medium [1]. Accompanied with the transparency feature, extreme dispersion of the EIT effects can significantly reduce the group velocity of light and offer promising applications in slow-light and nonlinear devices [2–5]. However, quantum EIT requires complicated experimental conditions, such as stable laser pumping and low temperature environment, which observably obstruct its implementations in practical applications.

Recently, various EIT-analogue optical systems, for instance coupled microresonators [6,7], optical waveguide [8–10], and metamaterials [11–13], have been drawn great attention owing to their EIT-like behaviors which are similar to that of the quantum EIT system. These optical systems are more convenient for practical applications as they are all free from the stringent requirements of the experimental environment for quantum optics. Among these optical systems, metamaterial analogues of EIT have attracted great attention as they can easily realize EIT effects in the whole spectral range from microwave to ultraviolet [14–17] by defining a properly tailored geometry for the unit cell. Owing to their high transparency and

#364080 https://doi.org/10.1364/OE.27.016624
Journal © 2019 Received 2 Apr 2019; revised 16 May 2019; accepted 17 May 2019; published 29 May 2019

enhanced nonlinear properties, they have shown great potential in designing novel devices, such as optical modulators [18–20], optical buffers [21,22], and highly sensitive sensors [23–25].

Generally, EIT effects in these metamaterial analogues are realized by two approaches, 'bright-dark' model and 'bright-bright' model. The first one typically involves a narrow band 'bright' mode resonator, which can be efficiently coupled to the incident wave directly, and a broadband 'dark' mode resonator, which is not access to the incident wave but can be activated by the 'bright' mode resonator via near field coupling. When these two resonances are excited in close proximity in both the special and frequency domains, the Fano-type interference between them results in a narrow transmission or reflection window, and then EIT effects can be achieved [26–30]. The second approach has been rarely studied and reported. In this approach, two bright modes with comparable Q-factors are placed close to each other, and the frequency detuning and hybridization between them result in EIT effects [31–33]. Comparing to the former one, the second approach is much easier to be realized as both two bright modes can be directly excited by the incident wave.

However, most of these reported metamaterial analogues of EIT are realized based on plasmonic effects, which are limited by the large non-radiative ohmic loss on the metal surface. As a consequence, those plasmonic metamaterial analogues of EIT generally feature reduced Q-factor and modulation range [34]. Recently developed all-dielectric metamaterials offer a potential solution to this issue [35]. Multipoles with minimal absorption losses, including electric dipoles, magnetic dipoles, toroidal dipoles, and higher order Mie resonators, are excited in these high-refractive-index dielectric nanorenonators, and EIT effects can be realized based on the coupling between these nanorenonators. Moreover, these all-dielectric metamaterial analogues are significantly efficient when compared with their metallic counterparts [36–38]. For instance, in [36], authors reported a classical analogue of EIT using all-dielectric silicon-based metasurfaces. Based on coherent interaction between radiative and non-radiative resonators combined with the reduction of absorption loss, sharp EIT-like resonances with Q-factor up to ~483 was accomplished in the near-infrared regime.

In this paper, we propose a novel silicon-based metamaterial for EIT effects at terahertz frequencies. The unit cell of the proposed metamaterial consists of two asymmetric split ring resonators (a-SRR) whose asymmetric nature comes from the different lengths of their arcs. We demonstrate theoretically and then confirm experimentally that the proposed metamaterial can exhibit an EIT resonance with high transmittances, as well as large group delays, at frequencies around 0.78THz. Via numerical simulations, we show that the EIT transparent window in this system is aroused by the interaction between two bright modes, which are caused by the excitation of magnetic moments simultaneous in the same unit cell. We also confirm that, owing to the narrow linewidth of EIT resonance, the proposed metamaterial is promising for optical sensing applications with high sensitivity and figure-of-merit (FoM).

2. Design and characterization

Before the sample fabrication, we characterized optical properties of materials we prepared, including intrinsic silicon and polydimethylsiloxane (PDMS), using a standard terahertz time-domain spectroscopy (THz-TDS). The tested silicon sample is a ~100μm-thick silicon wafer, while the tested PDMS sample is a ~30μm-thick PDMS layer which is spin-coated on a silicon wafer with a 20mm × 20mm through hole at its center. The experimental results are shown in Fig. 1. We note that the measured refractive index is much higher that what was reported in [39] ($n_{PDMS} \sim 1.31$ at 0.8THz). This is because that the spin-coated PDMS layer had been baked at 120°C in an oven for 15min for the solidification.

As schematically demonstrated in Fig. 2(a), the unit cell of the proposed all-dielectric EIT metamaterial consists of two asymmetric split-ring resonators (a-SRRs) which are made of intrinsic silicon. The asymmetric nature of a-SRRs is resulted from the length difference of two $d = 100\mu m$ arcs, as the long arc spans α=160° and the short arc spans β=120°. To describe

Optics EXPRESS

the degree of asymmetry of a-SRRs, we define an asymmetric parameter $\eta=(\alpha-\beta)/(\alpha+\beta)\times100\%$, and for the proposed metamaterial η=14.3%. Meanwhile, the pair of SRRs in the unit cell is of mirror symmetry about the x-z plane, with the spacing between two SRRs is $d=50\mu m$. The SRRs are with height of $h=100\mu m$, outer radius of $R_1=75\mu m$, and inner radius of $R_2=37.5\mu m$. The periods of the unit cell in x- and y-directions are $P_x=400\mu m$ and $P_y=250\mu m$, respectively. The silicon SRRs are posted on a PDMS substrate with a thickness of $t=30\mu m$. The electromagnetic field excites the sample at normal incidence, with its electric field component parallel to the y-axis.

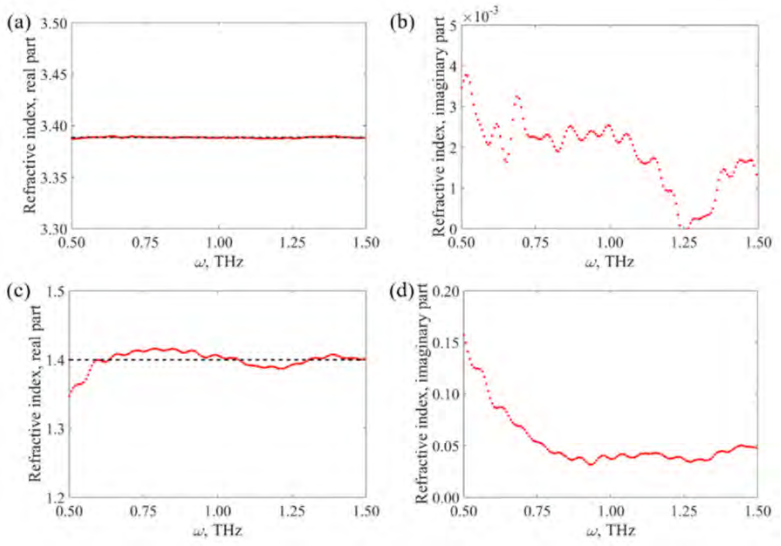

Fig. 1. Complex refractive index measured in the terahertz regime of (a) – (b) intrinsic silicon and (c) – (d) PDMS.

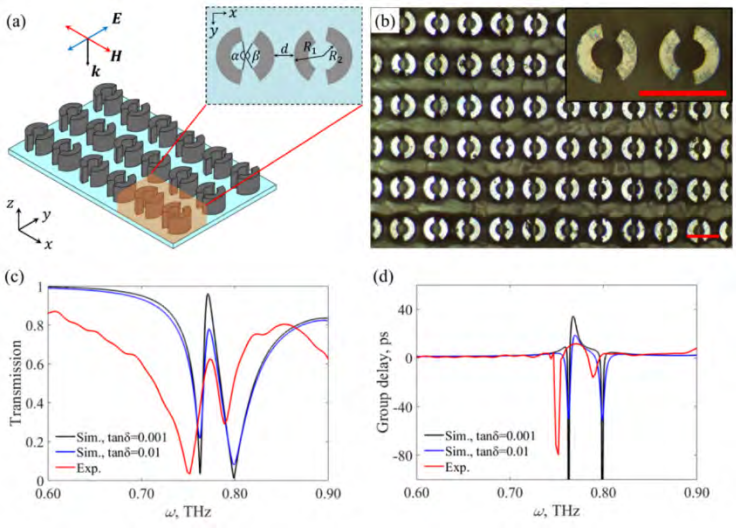

Fig. 2 (a) Schematic of the all-dielectric metamaterial composed of two asymmetric split ring resonators. Inset: top view of the unit cell. All dimensions shown here are $h=100\mu m$, $t=30\mu m$, $P_x=400\mu m$, $P_y=400\mu m$, $R_1=75\mu m$, $R_2=75\mu m$, $\alpha=160°$, and $\beta=120°$. (b) Microscopy of the fabricated sample. Bars refer to 500μm. (c) Transmission spectra and (d) corresponding group delay of the proposed metamaterial.

To characterize the optical properties of the proposed metamaterial, we firstly numerically simulated the transmission of the proposed metamaterial using a commercially available finite difference frequency-domain software package CST Microwave Studio. The simulated field transmission spectrum, and corresponding group delay which is retrieved from the complex transmission as $t_g = -\partial\varphi(\omega)/\partial\omega$ where $\varphi(\omega)$ is the phase shift of the transmitted THz wave, are plotted as solid red lines in Fig. 1(c) and (d), respectively. In these simulations, the Si resonators ($\varepsilon_{Si} = 11.7$) are sitting on a PDMS substrate (($\varepsilon_{PDMS} = 1.69$). A distinct EIT-like peak can be observed at the frequency of 0.78THz. The linewidth ($\Delta\omega$) of EIT resonances is evaluated by using a second moment method [40], which can be given by

$$\Delta\omega^2 = 4\frac{\int(\omega-\omega_0)^2 T(\omega)^2 d\omega}{\int T(\omega)^2 d\omega}, \quad (1)$$

where ω_c is the spectral position of EIT peak and $T(\omega)$ is the field transmission. To investigate the influence of material absorption, we performed simulations with different silicon material absorptions which were measured by the loss tangent. Although the curve shape has been changed, we find out that the material absorption would not effect on the spectral position and Q-factor of the EIT transparent peak. Based on simulation results we evaluated linewidths of simulated EIT peaks which are ~10.3GHz for both the low-loss silicon ($\tan\delta = 0.001$) and the high-loss silicon ($\tan\delta = 0.01$). The corresponding Q-factor, which can be defined as $Q = \omega_c/\Delta\omega$, is ~75.7. Furthermore, the group delay at the EIT resonant frequency reaches to 28.9ps and 18.3ps, respectively, leading to the potential of slow-light applications.

The designed metamaterial was fabricated by starting with a 100μm-thick intrinsic silicon wafer. A PDMS layer with a thickness of ~30μm was spin-coated on the back surface of the silicon wafer and was used as the substrate. The designed structure was patterned using the standard optical lithography followed by the deep reactive-ion etching with a Bosch process. The optical microscopy of the fabricated sample is shown in Fig. 2(b). Experimental measurements of THz transmission were performed in a dry gas pumped environment using the standard photoconductive-antenna based terahertz-time-domain spectroscopy (THz-TDS) system. During the measurements, the sample was illuminated by a normal-incident THz wave with the electric field oriented parallel to the split arrangement of SRRs. The experimentally measured transmittance and group delay were plotted as solid red lines in Fig. 2(c) and (d). A transmission peak with the transmittance of 63% can be observed at 0.773THz with a Q-factor of ~54.1. THz wave with central frequency of 0.773THz is delayed maximally by 11.7ps when propagating through the metamaterial device with a thickness of ~130μm (including the silicon posts and PDMS substrate), which corresponds to a propagating distance of ~3.5mm in free space. Although the material absorption of silicon, as shown by Fig. 1(b), is approximately similar to that of the low-loss silicon we used in simulations in the frequency range from 0.6THz to 0.9THz, experimental measurements show good agreement with numerical simulations for high-loss silicon. This phenomenon predicts that the material absorption has been increased due to the fabrication process. Inconsistencies in the shape of transmission curve and the Q-factor of EIT peak can be attributed to the distortion of the fabricated sample as the PDMS substrate is very flexible, which would introduce scattering losses and break coherence between the resonators.

3. Discussion

Firstly, we would like to investigate the physics behand the EIT-like behavior of the proposed metamaterial. In follow simulations, we use the low-loss silicon as the resonator material to reduce the influence of the material absorptions on electromagnetic responses. As schematically shown in Fig. 2(a), each unit cell of the proposed metamaterial can be regard as a

Optics EXPRESS

combination of a long-arc SRR subresonator and short-arc SRR subresonator which are placed fact-to-face. The EIT window of the proposed metamaterial is due to the interaction between these two subresonators. In Fig. 3(a), we provide the transmission spectrum of the

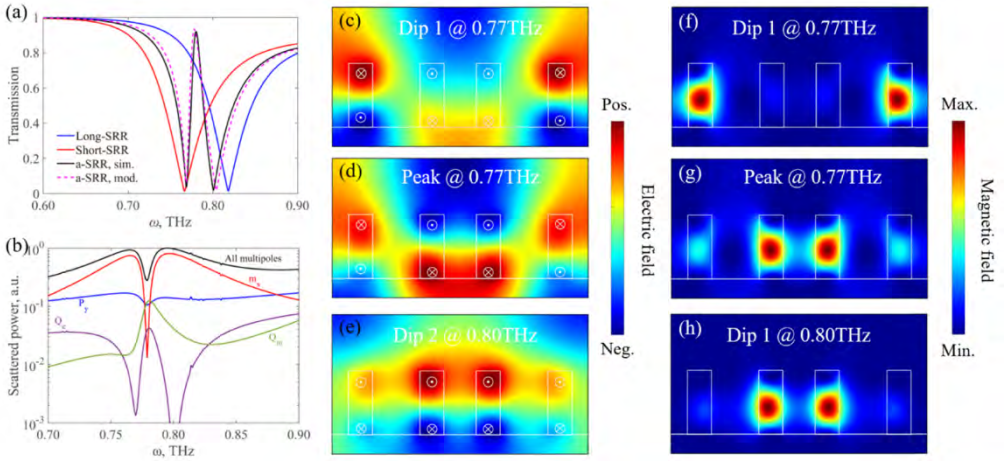

Fig. 3. (a) Simulated transmission curves of Short SRR (blue solid line), long SRR (red solid line), and a-SRR (black solid line) metamaterials. The dashed magenta line refers the analytically fitted data using the two-oscillator model [Eq. (3)]. (b) Scattered power of the five major multipoles of the proposed metamaterial, including electric dipole (**P**), magnetic dipole (**M**), electric quadrupole $\mathbf{Q_e}$, and magnetic quadrupole $\mathbf{Q_m}$. Spatial distribution of (c)-(e) electric field and (f)-(h) magnetic field in the x-0-z plane bisecting the metamaterial at dip 1 (0.77THz), peak (0.78THz) and dip 2 (0.80THz), respectively.

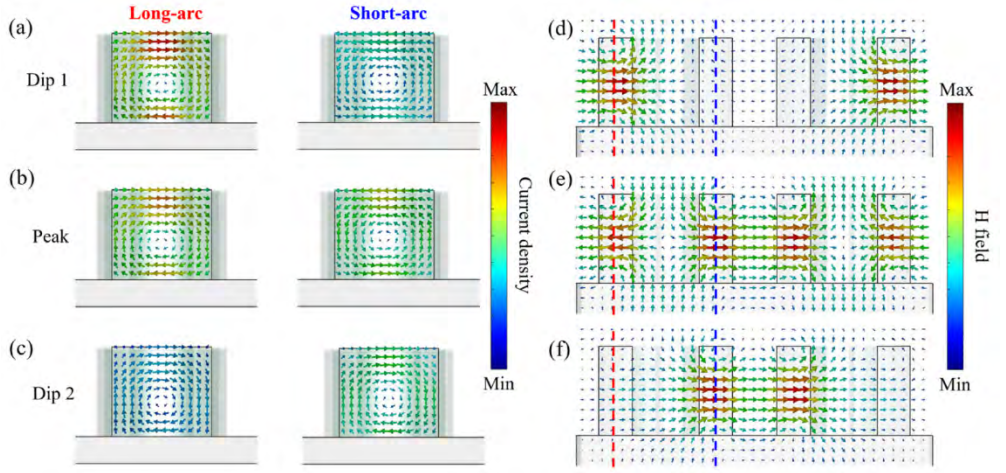

Fig. 4. Vector plots of magnetic fields at (a) Dip 1 0.77THz, (b) EIT peak 0.78THz, (c) Dip 2 0.80THz and (d) 0.776THz where the intensity of magnetic field is magnified by 5 times.

proposed a-SRR metamaterial (solid black line), which is superimposed with that of its two subresonators: short-SRRs (solid blue line) and long-SRRs (solid red line). It can be clearly observed that two transmission dips occurring at 0.77THz and 0.80THz inherit from the resonances associated with each individual subresonator, and the EIT peak appearing at 0.78THz is produced by the interaction between them. This behavior is further analyzed by simulating the spatial distribution of electric and magnetic fields at two transmission dips (dip 1 at 0.77THz and dip 2 at 0.80THz) and the transmission peak (at 0.78THz), respectively. The simulation results are depicted in Fig. 3(c) and (d). At transmission dips, two subresonators are excited successively. The induced electric field concentrates on top and bottom parts of

subresonators and circulates anticlockwise in the x-z plane, which predicts the formation of displacement current loops. The appearance of current loops can be expected for the excitation of magnetic moments which concentrate on central parts of subresonators. At the EIT transparency peak, two subresonators are simultaneously excited. But the induced magnetic moments in two subresonators, which are clearly depicted by vertical plots of magnetic field as shown in Fig. 4, are excited in opposite direction, and their interactions with the incident wave are clearly suppressed. This proves that the EIT transparency window of the proposed metamaterial is a consequence of the interaction between magnetic moments excited in two subresonators.

The electric and magnetic fields at resonant frequencies appear due to Mie-type modes, and the interaction between these modes results the EIT transparence window of the proposed metamaterial. To analyze the role of these modes in forming the EIT response, we calculate their relative strength in terms of the scattered electromagnetic power in the far-field zone. The multipole moments including electric dipole **P**, magnetic dipole **m**, electric quadrupole $\mathbf{Q_e}$, and magnetic quadrupole $\mathbf{Q_m}$, are calculated based in the density of induced displacement currents [38,41]. The calculation results are shown in Fig. 3(b). We note that excitations of magnetic dipole in two subresonators dominates all other standard multipoles at frequencies around two transmission dips. At frequencies around 0.78THz where the EIT peak appears, the excitation of magnetic dipole is strongly suppressed. Aside from magnetic dipole, other multipoles, including **P**, $\mathbf{Q_e}$ and $\mathbf{Q_m}$, are also excited, which contributes to widening the EIT peak and suppressing its Q factor due to radiating losses. We also note that the component-wise contributions of the induced dipole moments are oriented along the corresponding excitation fields. To be specific, **P** is excited along the y-axis, while **m** is parallel to the x-axis.

Furthermore, we also study qualitatively the response of the proposed metamaterial by applying the coupled harmonic oscillator model, which can be described as [33,42]:

$$\begin{aligned} &\ddot{x}_a(t)+\gamma_a\dot{x}_a(t)+\omega_a x_a(t)+\Omega^2 x_b(t)=c_a E \\ &\ddot{x}_b(t)+\gamma_b\dot{x}_b(t)+\omega_b x_b(t)+\Omega^2 x_a(t)=c_b E \end{aligned} \tag{2}$$

Here, long arc subresonators and short arc subresonators are described as particles *a* and *b*, respectively. (ω_a, ω_b) and (γ_a, γ_b) are resonance angular frequencies and damping strengths, and Ω refers to the coupling coefficient between two subresonators. c_a and c_b are the coupling efficiency between the individual subresonator and the indicant THz wave $E = E_0 \exp(i\omega t)$ respectively. The effective susceptibility χ_{eff} of the EIT structure, which is proportional to the ratio of the polarization ($\boldsymbol{P}$) of the particles to the strength of incident electric field ($\boldsymbol{E}$), can be obtained by solving the displacement vectors of two SRRs from Eq. (2):

$$\begin{aligned} \chi_{eff} &= \frac{\boldsymbol{P}}{\varepsilon_0 \boldsymbol{E}} = \frac{c_a x_a + c_b x_b}{\varepsilon_0 \boldsymbol{E}} \\ &= K \times \left[\frac{c_a^2\left(\omega^2-\omega_b^2\right)+c_b^2\left(\omega^2-\omega_a^2\right)+c_a c_b \Omega}{\Omega^4-\left(\omega^2-\omega_a^2+i\omega\gamma_a\right)\left(\omega^2-\omega_b^2+i\omega\gamma_b\right)} \right. \\ &\quad \left. i\omega \frac{c_a^2\gamma_b+c_b^2\gamma_a}{\Omega^4-\left(\omega^2-\omega_a^2+i\omega\gamma_a\right)\left(\omega^2-\omega_b^2+i\omega\gamma_b\right)} \right] \end{aligned} \tag{3}$$

where *K* is a proportionality factor. According to the Kramers-Kronig relations, the transmission coefficient can be given by $\mathbf{T} = 1 - \mathbf{A}$ where $\mathbf{A} = \mathrm{Im}(\chi_{eff})$ is the absorption losses in the sample. In our fitting, ω_a and ω_b are set as $2\pi \times 0.77 \times 10^{12} rad/s$ and $2\pi \times 0.80 \times 10^{12} rad/s$, respectively; the loss factors of two SRRs are obtained from the

linewidth of simulated transmission curve, and calculated as $5.61\times10^{11} rad/s$ and $7.91\times10^{11} rad/s$. The dashed magenta line in Fig. 2(a) demonstrates the analytically modeled transmission spectra using Eq. (3). Although there are minor differences in amplitude and bandwidths for the spectra in Fig. 1(c), the analyzed model shows very good agreements with the simulated results.

As demonstrated above, the EIT resonance of the proposed metamaterial is resulted from the interaction between two subresonators. Thus, the coupling coefficient, Ω, plays an important role in forming a high-Q-factor EIT resonance. We characterize the spectral response of the proposed metamaterial with respect to the spacing between two SRRs *d* which is changed by shifting two subresonators simultaneously. As schematically demonstrated in Fig. 5(c), with a larger spacing between two SRRs, the spacing between long-arc and short-arc subresonators, as well as the coupling distance these two subresonators, is reduced. In Fig. 5(a), we show transmission spectra of metamaterial with different spacing between two SRRs which increases from 110μm to 150μm. The enlarging of coupling distance leads to redshifts of EIT resonant frequency. The local distributions of magnetic field as EIT resonant frequencies, as shown in Fig. 5(b), help further understand the physics behand the formation of EIT peak and its response to the variation of subresonator spacing. A weak localization of magnetic field at the long arc resonators can be observed for larger subresonator spacing. The coupling coefficient Ω, which evaluate the strength of coupling between two subresonators, is extracted from the analytical fit using the fitting model descripted by Eq. (2) – (3) to simulated transmission spectra of metamaterials with different SRRs spacing. For comparison, we also retrieved Q-factors of numerically simulated and analytically modeled EIT peaks using Eq. (1), as depicted in Fig. 5(d). In addition, we also studied transmission spectrum evolution in terms of arc length. In Fig. 5, we present electromagnetic response of the proposed metamaterial with different lengths of short-arc-subresonators, which varies from $\beta = 70°$ to $\beta = 140°$. Clearly, with shorter lengths of short-arc-subresonators, EIT peaks are broadened and localizations of magnetic field in long-arc-subresonators are restrained, which provide weakening the coupling between two subresonators, and decreasing of Q-factor. As shown in Fig. 5(d) and 6(d), we can easily conclude that Q-factor of EIT peak is inversely proportional to Ω, which agree with results shown in [11].

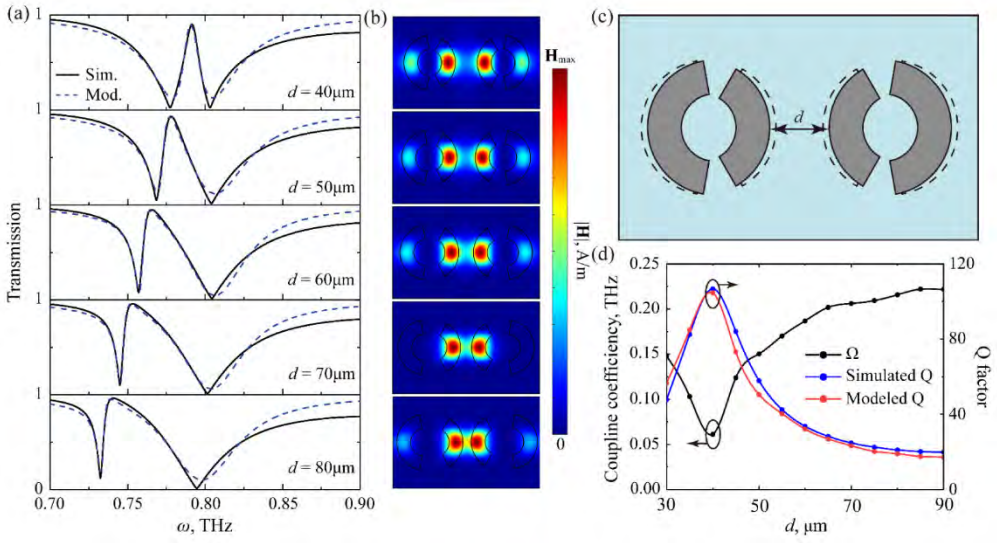

Fig. 5. (a) Numerically simulated (solid black lines) and analytically modeled (dashed blue lines) transmission spectra for the proposed metamaterial with different spacing between two SRRs. (b) Local H-field maps for the unit cell with varying SRRs spacing. (c) Schematic

Optics EXPRESS

showing the variation of the SRRs spacing. The dashed lines show original positions of subresonators in the proposed metamaterial with $d = 150\mu m$. (d) Extracted coupling coefficient and Q factor as a function of the SRRs spacing.

Due to their narrow linewidth, one potential application the EIT effects of the proposed metamaterial is the THz sensing. As a demonstration, we study the proposed a-SRR metamaterial with different background refractive indices. The simulated transmittance spectra with background refractive indices varying from 1.0 to 1.4 are presented in Fig. 7. One can clearly observe a substantial shift of the EIT peak position is realized by small refractive index changes. The EIT peak position keeps moving to lower frequencies till the surround refractive index reaches to 1.4. By fitting the shift of the EIT peak position, we obtain the sensitivity of the proposed metamaterial, which is measured by the shift of resonance per refractive-index-unit (RIU) changes, as $S = 231\text{GHz} / \text{RIU}$. Besides the sensitivity, the sensing performance of the proposed metamaterial can also be characterized by the figure-of-merit (FoM), which can be defined by the sensitivity (S) and the linewidth of the resonance ($\Delta\omega$) as $\text{FoM} = S / \Delta\omega$. When the background refractive indices vary from 1.0 to 1.4, the average linewidth of EIT resonances is about 18.2GHz, leading to a FoM of 12.7. With such a high sensitivity and high FoM, the proposed metamaterial can be used as a THz sensor for identifying various gaseous and aerosol analytes or measuring the concentration of dust particles in the air.

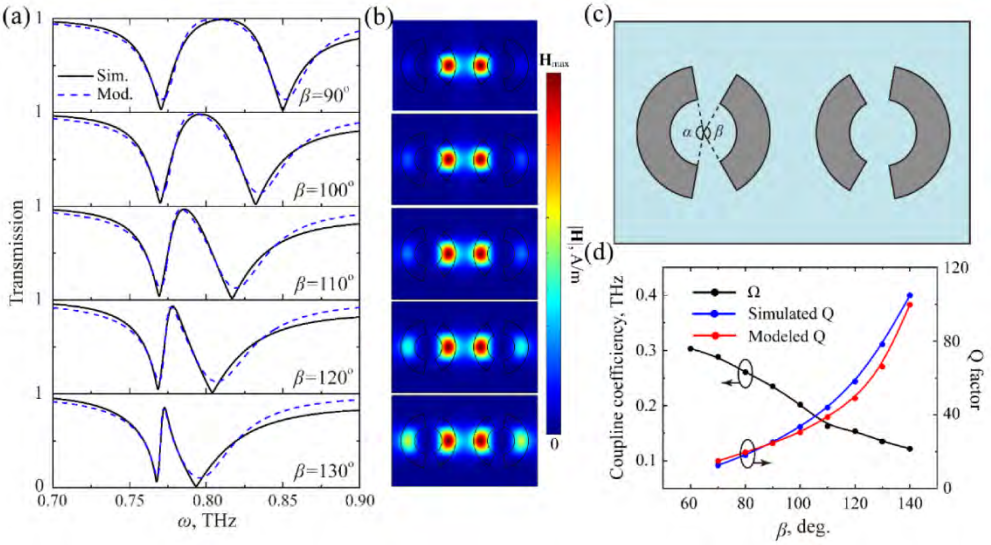

Fig. 6. (a) Numerically simulated (solid black lines) and analytically modeled (dashed blue lines) transmission spectra for the proposed metamaterial with different lengths of short-arc-subresonator. (b) Local H-field maps for the unit cell with varying length of short-arc-subresonator. (c) Schematic showing the variation of the subresonator spacing. (d) Extracted coupling coefficient and Q factor as a function of length of short-arc-subresonator.

Finally, we would like to compare EIT-resonant and sensing performances of the proposed metamaterial with other types of metamaterial-based sensing devices. The Q-factor and FoM of our metamaterial is comparable to the best records of plasmonic EIT metamaterials [30–33], but is not as large as that exhibited by dielectric EIT metamaterials working in the visible and infrared range [36–38]. We should claim that the sensing performance of our metamaterial can be further improved via optimizing its structure. In Fig. 8(a), we demonstrate a sample that the metamaterial with an optimized structure can exhibit an EIT peak with a linewidth of 3.5GHz and a Q-factor of ~270. We also investigate its sensing capacity by simulating its transmission spectra with different surround refractive index. When the surround refractive index varies

Optics EXPRESS

from 1.0 to 1.4, the EIT resonant frequency shifts from 0.94THz to 0.85THz, resulting a sensitivity of 226GHz/RIU. The relevant FoM can reaches to ~64.7 when the surround refractive index is 1.0.

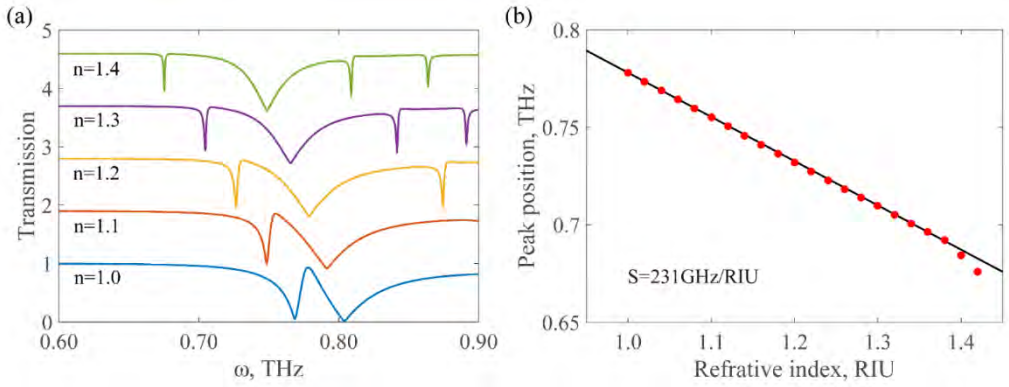

Fig. 7. (a) Simulated transmittance spectra of the proposed metamaterial when the background refractive indices varying from 1.0 to 1.4. (b) The spectral position of the EIT peak as a function of the background refractive index. The linear fit (solid black line) reveals the sensitivity as S = 231GHz / RIU.

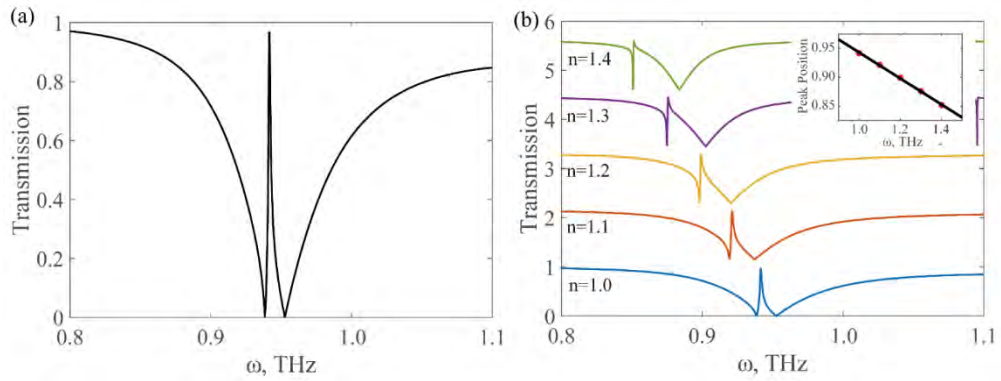

Fig. 8. (a) Simulated transmission spectrum of the EIT metamaterial with an optimized structure. Its structural parameters are as follows: $h = 100\mu m$, $t = 30\mu m$, $P_x = 320\mu m$, $P_y = 320\mu m$, $R_1 = 60\mu m$, $R_2 = 40\mu m$, $\alpha = 160°$, and $\beta = 140°$. (b) Simulated transmittance spectra of the optimized metamaterial when the background refractive indices varying from 1.0 to 1.4. Inset: The spectral position of the EIT peak as a function of the background refractive index.

4. Conclusion

A dielectric metamaterial analogue of EIT is for applications in the terahertz frequency range. The unit cell of the proposed EIT metamaterial consists of two a-SRRs positioned in a mirror symmetry. The asymmetric nature of SRRs results from the different lengths of individual arcs, as the long arcs span $\alpha = 160°$ while the short arcs span $\beta = 120°$. Simulation results revealed that the proposed metamaterial exhibited an EIT-like transmittance window with a Q-factor of ~75.7 in the frequency range around 0.780THz. Based on the proposed metamaterial structure, we fabricated a sample comprising of silicon resonators and PDMS substrate by using standard lithography followed by reactive-ion-itching. Transmittances of the fabricated sample was characterized by standard THz-TDS system with dry-gas pumping. We observed an EIT resonance peaked at 0.773THz, featuring a Q-factor of ~54.1. The location

and Q-factor of the measured EIT resonance are in good agreement with theoretical predictions. We also confirmed that our metamaterial can be used as an optical sensor for monitoring the background refractive indices. Its sensitivity and FoM reach to 231GHz/RIU and ~12.7, respectively, and can be further improved by optimizing its structure. The high sensitivity and FoM of the proposed metamaterial guarantee its potential applications in in situ chemical and biological detection.

Funding

National Natural Science Foundation of China (51627901 and 11704373), the National Key Research and Development Program of China, the Bureau of Facility Support and Budget, CAS, the Ministry of Science and Technology (2016YFA0401004, 2017YFA0402904), the Chinese Universities Scientific Fund (WK2340000071, WK2310000076), and Anhui Initiative in Quantum Information Technologies (AHY100000).

Acknowledgments

The device fabrication in this work was partially carried out at the USTC Center for Micro and Nanoscale Research and Fabrication.

References

1. K. Boller, A. Imamolu, and S. E. Harris, "Observation of electromagnetically induced transparency," Phys. Rev. Lett. **66**(20), 2593–2596 (1991).
2. L. V. Hau, S. E. Harris, Z. Dutton, and C. H. Behroozi, "Light speed reduction to 17 metres per second in an ultracold atomic gas," Nature **397**(6720), 594–598 (1999).
3. I. Novikova, R. L. Walsworth, and Y. Xiao, "Electromagnetically induced transparency-based slow and stored light in warm atoms," Laser Photonics Rev. **6**(3), 333–353 (2012).
4. H. Schmidt and A. Imamogdlu, "Giant Kerr nonlinearities obtained by electromagnetically induced transparency," Opt. Lett. **21**(23), 1936–1938 (1996).
5. Y. Zhang, A. W. Brown, and M. Xiao, "Opening four-wave mixing and six-wave mixing channels via dual electromagnetically induced transparency windows," Phys. Rev. Lett. **99**(12), 123603 (2007).
6. D. D. Smith, H. Chang, K. A. Fuller, A. Rosenberger, and R. W. Boyd, "Coupled-resonator-induced transparency," Phys. Rev. A **69**(6), 063804 (2004).
7. Q. Xu, S. Sandhu, M. L. Povinelli, J. Shakya, S. Fan, and M. Lipson, "Experimental realization of an on-chip all-optical analogue to electromagnetically induced transparency," Phys. Rev. Lett. **96**(12), 123901 (2006).
8. X. Yang, M. Yu, D. L. Kwong, and C. W. Wong, "All-optical analog to electromagnetically induced transparency in multiple coupled photonic crystal cavities," Phys. Rev. Lett. **102**(17), 173902 (2009).
9. M. F. Yanik, W. Suh, Z. Wang, and S. Fan, "Stopping light in a waveguide with an all-optical analog of electromagnetically induced transparency," Phys. Rev. Lett. **93**(23), 233903 (2004).
10. H. Lu, X. Liu, and D. Mao, "Plasmonic analog of electromagnetically induced transparency in multi-nanoresonator-coupled waveguide systems," Phys. Rev. A **85**(5), 053803 (2012).
11. S. Zhang, D. A. Genov, Y. Wang, M. Liu, and X. Zhang, "Plasmon-induced transparency in metamaterials," Phys. Rev. Lett. **101**(4), 047401 (2008).
12. N. Papasimakis, V. A. Fedotov, N. I. Zheludev, and S. L. Prosvirnin, "Metamaterial analog of electromagnetically induced transparency," Phys. Rev. Lett. **101**(25), 253903 (2008).
13. N. Liu, L. Langguth, T. Weiss, J. Kästel, M. Fleischhauer, T. Pfau, and H. Giessen, "Plasmonic analogue of electromagnetically induced transparency at the Drude damping limit," Nat. Mater. **8**(9), 758–762 (2009).
14. L. Zhu, F. Y. Meng, L. Dong, Q. Wu, B. J. Che, J. Gao, J. Fu, K. Zhang, and G. Yang, "Magnetic metamaterial analog of electromagnetically induced transparency and absorption," J. Appl. Phys. **117**(17), 17D146 (2015).
15. R. Singh, C. Rockstuhl, F. Lederer, and W. Zhang, "Coupling between a dark and a bright eigenmode in a terahertz metamaterial," Phys. Rev. B Condens. Matter Mater. Phys. **79**(8), 085111 (2009).
16. R. Maas, J. van de Groep, and A. Polman, "Planar metal/dielectric single-periodic multilayer ultraviolet flat lens," Optica **3**(6), 592–596 (2016).
17. S. Biswas, J. Duan, D. Nepal, K. Park, R. Pachter, and R. A. Vaia, "Plasmon-induced transparency in the visible region via self-assembled gold nanorod heterodimers," Nano Lett. **13**(12), 6287–6291 (2013).
18. H. Chen, W. J. Padilla, M. J. Cich, A. K. Azad, R. D. Averitt, and A. J. Taylor, "A metamaterial solid-state terahertz phase modulator," Nat. Photonics **3**(3), 148–151 (2009).
19. J. He, P. Ding, J. Wang, C. Fan, and E. Liang, "Ultra-narrow band perfect absorbers based on plasmonic analog of electromagnetically induced absorption," Opt. Express **23**(5), 6083–6091 (2015).
20. G. R. Keiser, N. Karl, P. Q. Liu, C. Tulloss, H. T. Chen, A. J. Taylor, I. Brener, J. L. Reno, and D. M. Mittleman, "Nonlinear terahertz metamaterials with active electrical control," Appl. Phys. Lett. **111**(12), 121101 (2017).

Optics EXPRESS

21. T. Nakanishi, T. Otani, Y. Tamayama, and M. Kitano, "Storage of electromagnetic waves in a metamaterial that mimics electromagnetically induced transparency," Phys. Rev. B Condens. Matter Mater. Phys. **87**(16), 161110 (2013).
22. M. Liu, Q. Yang, Q. Xu, X. Chen, Z. Tian, J. Gu, C. Ouyang, X. Zhang, J. Han, and W. Zhang, "Tailoring mode interference in plasmon-induced transparency metamaterials," J. Phys. D Appl. Phys. **51**(17), 174005 (2018).
23. Y. Tian, S. Hu, X. Huang, Z. Yu, H. Lin, and H. Yang, "Low-loss planar metamaterials electromagnetically induced transparency for sensitive refractive index sensing," J. Phys. D Appl. Phys. **50**(40), 405105 (2017).
24. D. B. Litt, M. R. Jones, M. Hentschel, Y. Wang, S. Yang, H. D. Ha, X. Zhang, and A. P. Alivisatos, "Hybrid lithographic and DNA-directed assembly of a configurable plasmonic metamaterial that exhibits electromagnetically induced transparency," Nano Lett. **18**(2), 859–864 (2018).
25. Y. Song, H. Zhan, C. Jiang, K. Zhao, J. Zhu, R. Chen, S. Hao, and W. Yue, "High water content prediction of oil–water emulsions based on terahertz electromagnetically induced transparency-like metamaterial," ACS Omega **4**(1), 1810–1815 (2019).
26. R. Singh, C. Rockstuhl, F. Lederer, and W. Zhang, "Coupling between a dark and a bright eigenmode in a terahertz metamaterial," Phys. Rev. B Condens. Matter Mater. Phys. **79**(8), 085111 (2009).
27. M. Manjappa, S. P. Turaga, Y. K. Srivastava, A. A. Bettiol, and R. Singh, "Magnetic annihilation of the dark mode in a strongly coupled bright-dark terahertz metamaterial," Opt. Lett. **42**(11), 2106–2109 (2017).
28. K. M. Devi, A. K. Sarma, D. R. Chowdhury, and G. Kumar, "Plasmon induced transparency effect through alternately coupled resonators in terahertz metamaterial," Opt. Express **25**(9), 10484–10493 (2017).
29. S. Xiao, T. Wang, T. Liu, X. Yan, Z. Li, and C. Xu, "Active modulation of electromagnetically induced transparency analogue in terahertz hybrid metal-graphene metamaterials," Carbon **126**, 271–278 (2018).
30. Z. Xu, S. Liu, S. Li, and X. Yin, "Analog of electromagnetically induced transparency based on magnetic plasmonic artificial molecules with symmetric and antisymmetric states," Phys. Rev. B **99**(4), 041104 (2019).
31. M. Parvinnezhad Hokmabadi, E. Philip, E. Rivera, P. Kung, and S. M. Kim, "Plasmon-induced transparency by hybridizing concentric-twisted double split ring resonators," Sci. Rep. **5**(1), 15735 (2015).
32. H. Chen, H. Zhang, M. Liu, Y. Zhao, X. Guo, and Y. Zhang, "Realization of tunable plasmon-induced transparency by bright-bright mode coupling in Dirac semimetals," Opt. Mater. Express **7**(9), 3397–3407 (2017).
33. R. Yahiaoui, J. A. Burrow, S. M. Mekonen, A. Sarangan, J. Mathews, I. Agha, and T. A. Searles, "Electromagnetically induced transparency control in terahertz metasurfaces based on bright-bright mode coupling," Phys. Rev. B **97**(15), 155403 (2018).
34. B. Luk'yanchuk, N. I. Zheludev, S. A. Maier, N. J. Halas, P. Nordlander, H. Giessen, and C. T. Chong, "The Fano resonance in plasmonic nanostructures and metamaterials," Nat. Mater. **9**(9), 707–715 (2010).
35. I. Staude and J. Schilling, "Metamaterial-inspired silicon nanophotonics," Nat. Photonics **11**(5), 274–284 (2017).
36. Y. Yang, I. I. Kravchenko, D. P. Briggs, and J. Valentine, "All-dielectric metasurface analogue of electromagnetically induced transparency," Nat. Commun. **5**(1), 5753 (2014).
37. L. Zhu, X. Zhao, L. Dong, J. Guo, X. J. He, and Z. M. Yao, "Polarization-independent and angle-insensitive electromagnetically induced transparent (EIT) metamaterial based on bi-air-hole dielectric resonators," RSC Advances **8**(48), 27342–27348 (2018).
38. B. Han, X. Li, C. Sui, J. Diao, X. Jing, and Z. Hong, "Analog of electromagnetically induced transparency in an E-shaped all-dielectric metasurface based on toroidal dipolar response," Opt. Mater. Express **8**(8), 2197–2207 (2018).
39. A. Podzorov and G. Gallot, "Low-loss polymers for terahertz applications," Appl. Opt. **47**(18), 3254–3257 (2008).
40. A. E. Siegman, G. Nemes, and J. Serna, "How to (maybe) measure laser beam quality," in *DPSS (Diode Pumped Solid State) Lasers: Applications and Issues* (Optical Society of America, 1998), p. MQ1.
41. V. Savinov, V. A. Fedotov, and N. I. Zheludev, "Toroidal dipolar excitation and macroscopic electromagnetic properties of metamaterials," Phys. Rev. B Condens. Matter Mater. Phys. **89**(20), 205112 (2014).
42. F. Zhang, S. Feng, K. Qiu, Z. Liu, Y. Fan, W. Zhang, Q. Zhao, and J. Zhou, "Mechanically stretchable and tunable metamaterial absorber," Appl. Phys. Lett. **106**(9), 091907 (2015).